Calcinable Polymer Membrane with Revivability for Efficient Oily Water Remediation

Zhigao Zhu, Wei Wang, Dianpeng Qi, Yifei Luo, Yuanren Liu, Ying Xu, Fuyi Cui, Ce Wang, Xiaodong Chen**

Dr. Z. Zhu, Prof. W. Wang, Y. Liu, Dr. Y. Xu
State Key Laboratory of Urban Water Resource and Environment, School of Environment, Harbin Institute of Technology, Harbin 150090, P. R. China.
E-mail: wangweirs@hit.edu.cn

Dr. D. Qi, Y. Luo, Prof. X. Chen
Innovative Centre for Flexible Devices (iFLEX), School of Materials Science and Engineering, Nanyang Technological University, 50 Nanyang Avenue, 639798, Singapore.
E-mail: chenxd@ntu.edu.sg

Prof. F. Cui
College of Urban Construction and Environmental Engineering, Chongqing University, Chongqing 400044, P. R. China.

Prof. C. Wang
Alan G. Macdiarmid Institute, College of Chemistry, Jilin University, Changchun 130012, P. R. China.

Keywords: Calcinable polymer membrane; revivable membrane; oily water remediation; composite materials; electrospinning

Abstract: Fouling of polymeric membranes remains a major challenge for long-term operation of oily water remediation. The common reclamation methods to recycle fouled membranes have the issues of either imcomplete degradation of organic pollutants or damage to filter membranes. In this work, we report a calcinable polymer membrane with effective reclamation after fouling, which shows fully recovering the original oil/water separation efficiency. The membrane is made of polysulfonamide/polyacrylonitrile fibers by emulsion electrospinning, followed by hydrothermal decoration of TiO_2 nanoparticles. The bonding structured fibrous

membrane displays outstanding thermal stability in air (400 °C), strong acid/alkali resistance (at the pH range from 1 to 13), and robust tensile strength. As a result, the chemically fouled polymeric membrane can be easily reclaimed without decreasing in separation performance and mechanical property by annealing treatment. As a proof-of-concept, we integrated the as-prepared membrane into a wastewater separation tank, which achieves a high water flux over 3000 $L/m^2 \cdot h$ and oil rejection efficiency of 99.6% for various oil-in-water emulsions. The presented strategy on membrane fabrication is believed an effective remedy for membrane fouling, and should apply in a wider field of filtration industry.

Oily water remediation is critical to modern society, since the oily water generated from domestic activities, industrial processes and marine oil spills, takes heavy tolls on global environment and human health.[1-4] Common methods to treat oily water include skimmers, air flotation, coagulation-flocculation, centrifugation, depth filters and membrane filtration.[5-8] Among them, membrane-based oil/water separation, working on the basis of selective surface wettability, excelled itself in high efficiency, low cost, simple operation and energy-saving.[9-15] Currently, polymeric membranes for oily water remediation draw special interest due to their light weight, mechanical flexibility, desired shapes and easy integration.[1,4,16]

However, fouling of the polymeric membranes greatly impaired their applications.[17] Even the underwater antifouling membrane has to suffer from fouling by polar organics in water (e.g. humic acids, polyoses, proteins and bio-films) during

long-term operation (generally several days),[11,13,18] resulting in gradual decrease in the flux and separation efficiency. The most widely used route to regenerate fouled polymeric membranes is chemical rinsing with strong oxidants, which however, would bring about membrane corrosion, destroyed selective wettability and shortened membrane life.[19] Photocatalysis is another common method to treat fouled membranes, where organic pollutants degrade when exposed to visible or ultraviolet light irradiation.[20-23] However, photocatalysis under irradiation would generate photo-corrosion on the polymers by free radical reactions. Furthermore, it is unable to completely mineralize the contaminants, leaving organic residues on the membranes.[24,25] Therefore, fouling is still a big challenge that limits the application of polymeric membranes for oily water remediation.

Pyrolysis is the most effective and facile method to degrade organic matters, since most organics could be radically degraded at a certain high temperature in atmosphere.[26-28] Thus, if a calcinable and selectively-wettable polymeric separator is constructed, the polymeric membrane technology would be endowed with a revivable feature to maintain high performance of oily water remediation. Polysulfonamide (PSA) as a kind of special engineering plastics (SEPs), possesses unique sulfone groups in main chain that enhance the electron conjugation of benzene rings with NHCO groups, thereby leading to excellent thermal property and chemical resistance.[29,30] Moreover, the abundant NHCO polar groups endows PSA with much better hydrophilicity than other SEPs (Figure S1, Supporting Information).[31]

Therefore, PSA should be a good candidate with calcinable property for oily water remediation.

In the present work, we rationally fabricated a thermally stable filtration membrane based on inter-bonding structured PSA fibers with anchored TiO_2 nanoparticles (NPs) via an emulsion electrospinning method. The formation of the inter-bonding structure in the fibers doubled the tensile strength of the membrane. The hierarchically structured TiO_2 NPs decorating on the fibrous substrate enabled the membrane with intriguing superhydrophilicity (water contact angle (WCA) of 0°) and underwater superoleophobicity (underwater oil contact angle (UOCA) of 155°). Most importantly, the fouled membrane (by model extracellular polymeric substances, EPS) could be easily reclaimed by calcination at 400 °C. Even after 10 cycles of reclamations, no degradation of the filtration performance was observed. Finally, the as-prepared membrane was employed for oily water remediation and a high water flux over 3000 $L/m^2 \cdot h$ and rejection efficiency of 99.6% for various oil-in-water emulsions were achieved, which was comparable to the previous results.

PSA fibrous filtration matrix was fabricated by electrospinning technique, since electrospun products are advantageous in filtrate flux due to the interconnected porous structure and high porosity.[32-36] The formation of pure PSA fibers via electrospinning was relatively difficult. As observed from Scanning Electron Microscope (SEM) images in Figure S2 (Supporting Information), the diameter of the pure PSA fibers was nonuniform, possibly because of the poor spinnability and instable Taylor corn during electrospinning. Additionally, the droplets were easily splashed onto the

resultant membrane surface, destroying the samples (Figure S2d, Supporting Information). Therefore, polyacrylonitrile (PAN) acting as an assistant polymer was added into PSA solution to obtain uniform and bonding structured PSA fibrous membrane (FM). As shown in **Figure 1**a-c, the pure PSA and PAN electrospinning solutions are transparent with the turbidity of 58 and 48 nephelometric turbidity unit (NTU), respectively. In contrast, the composite PSA/PAN solution (mass ratio: 9/1) appears more turbid (66 NTU). Figure 1c presents the optical micrograph of PSA/PAN solution, in which micelles are dispersed. The presence of micelles can be attributed to the compatibility difference of the two polymers in *N,N*-dimethylacetamide (DMAc) solvent. Freezing SEM-EDX mapping image of the dispersion phase in PSA/PAN emulsion solution was characterized to verify the component as shown in Figure S3 (Supporting Information). Obviously, the sulfur (S) element of PSA is uniformly dispersed on the dispersion phase surface. Because there was no S element in PAN, the unique S element indicates that the dispersion phase should be PSA and the mother phase should be PAN. We believe that the emulsified non-homogeneous solution plays a key role in the formation of bonding structured PSA/PAN fibers. As schematically illustrated in Figure 1d, when continuous mother phase of PAN/DMAc undergoes electrospinning from Taylor cone tip, PSA/DMAc droplets in the dispersion phase are trapped at the cone base, and then stretched to form fiber under the electrostatic forces.[37] The good spinnability of PAN mother phase promotes the formation of PSA fibers. Most importantly, the solvent in dispersion phase (PSA/DMAC) encapsulated in the mother phase should overcome

the double handicap to evaporate during the electro-stretching process, which results in a small amount of residual solvent and facilitates the formation of bonding structured fibers.[38] High magnification SEM images of PSA (22 wt%) and PSA/PAN FMs fabricated from various polymer solutions at the fixed PSA to PAN ratio (9:1) are shown in Figure 1e and f and Figure S4a-e (Supporting Information). The morphology of composite fibers greatly changed after the introduction of PAN. Obvious adhesion structures could be observed among the adjacent fibers (Figure S4a, Supporting Information). When the polymer concentration was kept at a higher level (20 wt%), the high adhesion degree would block the fibrous membrane pores, making water penetration difficult (Figure S4a, Supporting Information). As the polymer concentration was below 12 wt%, bead-on-string structured fibers with poor mechanical properties were formed (Figure S4e, Supporting Information). Finally, the optimized PSA/PAN fibrous membrane (PSA:PAN = 9:1, 14 wt%) was made with uniform fiber diameters, bonding structures and without beads formation (Figure 1f and Figure S4d, Supporting Information). Notably, no bonding structures can be observed in pure PSA or pure PAN fibers, as shown in Figure 1e and Figure S2 and 4f (Supporting Information). To verify the dispersion of PSA in PSA/PAN fibers, X-ray Photoelectron Spectroscopy (XPS) survey spectrum and Fourier Transform Infrared Spectroscopy (FTIR) were used to study the composition of relevant fiber surfaces as shown in Figure S5, Figure S6 and Table S1 (Supporting Information). The S : C : N : O (atomic ratio) of the PSA fiber surface is found to be 3.03% : 74.65% : 6.76% : 15.56 %, respectively. However, after the introduction of PAN in PSA fibers, the

percentage of S atom was significantly decreased to 1.88%. The decreased S atomic ratio on the PSA/PAN fiber surface demonstrated that a certain amount of PAN was on the PSA/PAN fiber surface. This result also indirectly confirmed PSA/DMAc is the dispersion phase in the electrospinning emulsion.

The optimized PSA/PAN FM presents excellent thermal and mechanical properties. The thermal performance of PSA, PSA/PAN and PAN FMs were examined by a thermogravimetric analyzer (TGA) in N_2 atmosphere. As seen in Figure 1g, 0.82% of total weight lost at 100 °C is associated with the loss of moisture and solvent molecules bounded to the macromolecules. Following that, the PSA based FM could keep stable before 430 °C, while the PAN FM was sustainably decomposed after 280 °C. Finally, the weight is substantially lost in the high-temperature region of 430–600 °C because of the degradation of PSA backbones. These observations suggest the remarkable thermal stability of PSA/PAN FM. The tensile test results as shown in Figure 1h not only indicate the mechanical robustness of PSA/PAN FM, but also verify the inter-bonding structure. The coexistence of bonding/non-bonding parts in the PSA/PAN FM led to a nonlinear region and a subsequent linear region in the stress-strain curve, which can be explained by the two-step break mechanism as demonstrated in Figure 1i.[38,39] The non-bonding parts in the fibrous membrane could easily deform through slippage of fibers and were forced to be aligned along the stress direction when an external load was applied, resulting in the nonlinear elastic behavior in the first region. As the tensile stress further increased, the strain curve transformed into a linear elasticity until break with an extremely high linearity of

0.999 as indicated in Figure S7a (Supporting Information), which could be attributed to the elongation of individual PSA/PAN fibers. However, the as-prepared pure PAN and PSA FMs do not have bonding points, thus yield a larger slip strains with inferior linearity of PAN (0.979) and PSA (0.992) in stage 2. These phenomena suggest that the frictional slippage and elongation of PSA and PAN fibers without bonding-structures were simultaneously occurred in stage 2. In addition, Young's modulus is a parameter to reflect a material's resistance to elastic deformation. If the bonding points had formed among the adjacent fibers, a large modulus would be produced under a small stress. It could be calculated that the Young modulus of PSA/PAN FM (1.51 MPa) was far higher than that of pure PSA FM (0.47 MPa) and PAN FM (0.62 MPa) (Figure S7b, Supporting Information). Overall, the tensile strength of PSA/PAN FM (14.36 MPa) is almost twice that of PAN FM (6.26 MPa) and PSA FM (7.58 MPa). Since there was no obvious difference between the porosity of PSA/PAN FM (63.58%) and pure PSA FM (69.43%) (Supporting Information), the significant improvement in mechanical property should primarily come from the strengthening effect of the bonding structure.

In order to endow the filtration membrane with underwater superoleophobic surface and fast water permeation,[40-44] herein nano-scaled TiO_2 NPs were anchored on PSA/PAN fiber surface by hydrothermal modification for membrane roughness construction. The PSA/PAN FM was placed in an autoclave containing various dosages of tetrabutyl titanate (TBT).[45] After the hydrothermal synthesis at 180 °C for 12 h, TiO_2 NPs with an average diameter of around 15 nm were directly anchored

along the fiber axial direction as shown in **Figure 2**a. The composite fibrous membrane was denoted as TiO_2@PSA/PAN. The SEM, Transmission Electron Microscope (TEM) and 3D Atomic Force Microscope (AFM) images support the fact that the microstructures on the PSA/PAN fiber surface can be easily controlled by turning the dosage of TBT as shown in Figure 2a and b, and Figure S8 and 9 (Supporting Information). High-resolution TEM (HRTEM) analysis of the hybrid TiO_2@PSA/PAN reveals an interplanar distance of 0.35 nm for the (101) plane of TiO_2 as shown in the inset of Figure S9b (Supporting Information). The roughness of PSA/PAN fiber decorated by TiO_2 NPs was significantly improved from 81 to 268 nm as the TBT dosage increased from 0 to 0.4 mL, but was depressed to 142 nm with further increase of TBT to 0.8 mL. The TiO_2 NPs aggregate more easily in mother liquid at higher concentrations, making it difficult to stick onto the PSA/PAN fiber surface firmly (Figure S10, Supporting Information). N_2 ad/desorption was used to investigate the effect of TiO_2 NP content on surface roughness of the resultant TiO_2@PSA/PAN FMs (Figure S11a, Supporting Information). The specific surface areas of relevant TiO_2@PSA/PAN FMs are 6.13, 15.68, 28.76 and 17.37 m^2/g, respectively, indicating an obvious increase of surface area with TBT dosage increasing from 0 to 0.4 mL. However, when the TBT dosage was higher than 0.4 mL, a decrease in specific surface area occurred ranging from 28.76 to 17.37 m^2/g, which was in accordance with the studies of TEM and AFM images. Figure S11b (Supporting Information) indicates that the TiO_2@PSA/PAN FMs exhibited a typical mesoporous feature of size in the range of 10-120 nm with peak centred at 40 nm.

The as-prepared TiO_2@PSA/PAN FM presents outstanding selective wettability and fast water permeation after the above fabrication. As observed from Figure 2c and d, the TiO_2-0.4@PSA/PAN FM displays superamphiphilicity with both WCA and oil contact angle (OCA) of 0° in air when a water or oil droplet was placed onto the membrane surface. Interestingly, the oleophobicity (155°) appeared immediately when the oil droplet (trichloromethane) was placed into water on the fibrous membrane surface as shown in Figure 2d. The higher adhesion work of water than that of oil could be calculated from the Young-Dupré's equation: $W_{ad}=\gamma_{lv}(1+\cos\theta_{lv})$, where W_{ad} is the adhesion work, γ_{lv} is the surface tension of liquid, and θ_{lv} is the relevant liquid contact angle. The calculated W_{ad} of TiO_2-0.4@PSA/PAN FM (145.51 mN/m) was higher than that of oil (24.92 mN/m), demonstrating that it was difficult for oil to replace the infiltrated water in membrane.[46,47] Thus, the TiO_2-0.4@PSA/PAN FM exhibited low adhesion to an oil droplet with no permeation, whereas a water droplet could rapidly permeate through the membrane without any barrier. It was found that the UOCA was positively correlated to the membrane surface roughness. As shown in Figure 2e, the UOCA of the products raised from 129 to 155° as the TBT dosage was increased from 0 to 0.4 mL. Further increasing the TBT dosage to 0.8 mL would reduce the UOCA (144°). This can be explained by the formation of TiO_2 NP aggeragates (Figure S10, Supporting Information) at higher TBT dosage, decreasing the roughness of the composite fibers. The above results were in accordance with the TEM, AFM and Brunauer-Emmett-Teller (BET) results. The oil droplet adhesion ability and water droplet permeation process were captured

by a high-speed camera system. As shown in Figure 2f, an oil droplet (trichloromethane, 3 μL) was squeezed against the surface of TiO_2-0.4@PSA/PAN FM in water with an initial preload followed by a high load (for sufficient contact with the membrane surface). The oil droplet could depart from the membrane surface easily without obvious deformation at high load pressure, demonstrating extremely low oil adhesion. In contrast, when the TiO_2-0.4@PSA/PAN FM was contacted with a water droplet (3 μL) in air, the water permeated completely into the membranes within a short time (60 ms), illustrating the prominent superhydrophilic property and fast water adsorption of the resultant fibrous membrane.

The membrane displays ace stability in selevtive wettability even when subjected to corrosive liquids or anealing treatment. To evaluate the environmental stability, the UOCAs of fibrous membranes were tested in solutions of different pH values. As shown in Figure 2g, the membranes still maintain outstanding underwater superoleophobicity in strong alkali or acid conditions, exhibiting the excellent stability against corrosive conditions. In addition, benefiting from the high temperature resistance of PSA, the composite membrane presented a robust calcinable performance. A UOCA of 152^o was maintained even after annealing treatment at 400 °C for 1 h in air (Figure S12, Supporting Information).

Based on the above contact angle measurements, robust oil proofness, fast water flux, and effective oil/water separation were expected from the as-prepared composite membranes, and this is indeed the case. As presented in Figure 3a and Movie S1 (Supporting Information), the composite fibrous membrane exhibited a striking

resistance to oil droplets with hydrostatic oil pressure up to 70 kPa, which is beneficial for antifouling against oil during the separation process. To test the separation capacity of the as-prepared membrane, the TiO_2-0.4@PSA/PAN FM was fixed at the middle of the separation device as shown in Figure S13 (Supporting Information). 200 g of light oil mixture composed of n-hexane and water in a volume ratio of 1:1 was poured into the upper glass tube after the membrane was prewetted by water. Water could quickly pass through the membrane because of the excellent selective wettability, high porosity, and 3-dimensional open-cell network (Movie S2, Supporting Information). Meanwhile, the dyed oil was retained above the membrane due to the underwater superoleophobicity and low oil adhesion property. No external driving force except gravity was used during the fast separation process. The TiO_2-0.4@PSA/PAN FM exhibited a water flux of 7152 $L/m^2 \cdot h$ with high separation efficiency of 99.99 % (Movie S2, Supporting Information and Figure 3b), which was significantly higher than that of commercial hydrophilic polyvinylidene fluoride (PVDF) membrane (32 $L/m^2 \cdot h$, Figure 3d), mineral-coated polypropylene microfiltration membrane (90 $L/m^2 \cdot h$),[48] electropsun poly(m-phenylene isophthalamide) (PMIA) nanofibrous membrane (3311 $L/m^2 \cdot h$)[49] and polybenzoxazine/TiO_2 membrane coated mesh (3000 $L/m^2 \cdot h$)[50] solely driven by gravity (Table S2, Supporting Information).

Fouling of separation membranes is a common and tough issue during oily water treatment in real scenarios. An ideal membrane should possess both good antifouling property and recyclability.[51,52] Here, the antifouling performance against oil was

tested by detecting the water flux changes over TiO_2-0.4@PSA/PAN FM. The membrane exhibited an outstanding performance with nearly no flux decrease upon 10 cycles due to the excellent oil repelling performance (Figure 3b). As for oil/water mixture separation, the extracellular secretion of microorganism and polar organic impurity in real water body could block the membrane pores thus decreasing the UOCA and reducing the water flux. [52] These organic contaminants are hard to wash off by physical back flush. Alginates are usually employed as simulated polysaccharides that constitute a major fraction of EPS to investigate the membrane fouling mechanism.[53] Herein, 0.2 g of sodium alginate dissolved in 100 mL of oil/water mixture was employed to simulate the EPS product after long-term usage. Obvious decrease in water flux and reducing in UOCA took place, as shown in Figure 3c and d. A decrease in UOCA (112°) was due to the smoothing effect of the fiber surface by sodium alginate. For the calcinable performance, the fouled membrane could be directly reclaimed by annealing treatment at 400 °C for 1 h in air. The model EPS could be totally burned off and the UOCA can return to its original underwater superoleophobicity state with an UOCA of 152°. Most importantly, the retrieved membrane exhibited a high water flux of 8256 $L/m^2 \cdot h$, higher than that of pristine TiO_2-0.4@PSA/PAN FM (7152 $L/m^2 \cdot h$). In addition, the calcined TiO_2-0.4@PSA/PAN FM kept a high oil rejection efficiency of more than 99.99 %. This interesting phenomenon could be explained by the partial oxidation of PAN, which increased the dimension of microchannels and made water penetration easier. The color of the TiO_2-0.4@PSA/PAN FM turned from white to brown after annealing

treatment as shown in Figure 3e and f, confirming the partial carbonization of PAN. Images shown in Figure 3g and h suggest the calcined membrane still exhibited outstanding flexibility and intact fibrous structure with robust mechanical strength of 14.9 MPa (Figure S14, Supporting Information) after thermal reclamation. On the contrary, the commercial hydrophilic PVDF microporous membrane shrank significantly with a color change from white to transparent when treated at 180 °C in air for 5 min due to its low thermostability (Figure 3i).

The more intractable problem for oily water treatment is oil-in-water emulsion separation.[54,55] To test the emulsion separation capability of the as-prepared membranes, a continuous membrane separation tank for oil-in-water emulsion wastewater treatment was designed as shown in **Figure 4**a. The filtration membrane separated the wastewater tank and the clean water tank. The light oil after separation can float on the water surface at the top-left while the heavy oil can occupy the bottom of the tank and be discharged at the down-left. The pure water will be continuously collected in the clean water tank at the down-right. According to this design, an laboratory-scale equipment was set up shown in Figure 4b. An oily wastewater model composed of sodium dodecylbenzenesulfonate (SDBS) stabilized n-hexane-in-water emulsion was charged into the left wastewater tank. Then a transmembrane pressure of about 0.10±0.01 bar was applied to drive the separation process. The effluent amount grew linearly with time (Figure 4c). Around 170 mL of clean water was collected from the right tank within 5 min separation; thus the flux was calculated to be 3264 $L/m^2 \cdot h$ (Movie S3, Supporting Information). Figure 4d

displays a plausible mechanism for the oil-in-water emulsion separation. Upon touching the surface of the membrane, water immediately spreads and permeates into the membrane because of its preferential affinity with the membrane. Hence a stable water-solid interface is formed, which greatly enhanced the oil-proof pressure. Meanwhile, the small oil droplets quickly aggregate with each other to generate larger oil droplets, then leave the membrane surface and eventually float on the water surface according to the Stokes' law of resistance.[56] The images of the oil-in-water emusion and the corresponding collected filtrate are shown in Figure 4e and f. The collected filtrate was transparent and the UV-vis spectrum was flat compared to the original milky white feed emulsion, implying the TiO_2-0.4@PSA/PAN FM can effectively separate oil from oil-in-water emulsion. In addition, a series of oil-in-water emulsions (oil volume: 1%) based on isooctane, hexadecane, kerosene, hexane and petroleum were also prepared to test the separation performance. The fibrous membrane exhibited a fast water flux over 3000 $L/m^2 \cdot h$ and high separation effeciency over 99.6% as shown in Figure 4g, which is comparable with the results reported in literature (Table S2, Supporting Information).

In summary, a calcinable polymer membrane with revivablility for oliy water remediation was demonstrated. Benefiting from the electrospinning solution design and hierarchically structured TiO_2 NPs decoration on the fibrous substrate, the resultant composite TiO_2-0.4@PSA/PAN FM displayed intriguing superhydrophilicity (WCA of 0^o) and underwater superoelophobicity (UOCA of 155°), and was capable of separating oil/water mixture and various oil-in-water emulsions.

Besides, the membrane also displayed high thermal stability (400 °C), strong acid/alkali resistance (pH=1-13) and robust durability. Most importantly, the chemically fouled polymeric membrane could be easily reclaimed by annealing treatment without decrease in filtration performance and mechanical property. The present development provides a highly efficient and facile strategy for the preparation of revivable oil/water separation membrane. It is also expected to provide inspiration for the development of revivable membranes in other filtration fields, like microfiltration, ultrafiltration, distillation, reverse and forward osmosis for water treatment.

Experimental Section

Materials. PSA was purchased from Shanghai Tanlon Fiber Co., Ltd. PAN (M_w=90 000) was received from spectrum Chemicals & Laboratory Products Co., Ltd., USA. Tetrabutyl titanate (TBT), sodium alginate, *N,N*-dimethylacetamide (DMAc), isooctane, hexadecane, kerosene, petroleum, chloroform, n-hexane, absolute ethanol, sudan red G and methylene blue were obtained from Aladdin Chemical Reagents Co., Ltd., China. Milli-Q water with a resistance of 18.2 MΩ was obtained from Millipore system. All the reagents were of analytical grade and used as received without further purification.

Preparation of PSA and PSA/PAN FMs. The PSA concentrations of 20, 22, 24 and 26 wt% were prepared by dissolving PSA powder in DMAc with continuous stirring for

12 h. The PSA/PAN concentrations of 20, 18, 16, 14 and 12 wt% were prepared by dissolving PSA and PAN in DMAc with continuous stirring for 12 h and the weight ratio of PSA/PAN was fixed at 9:1. The solutions were electrospun at a fixed voltage of 12 kV and a feed rate of 1 mL/h with a work distance of 12 cm. The relevant temperature and humidity of electrospinning processes were fixed at 23±2 °C and 40±5%, respectively. The collected PSA/PAN FM dried at 60 °C in vacuum for 6 h. The obtained PSA FM fabricated from various concentrations of x wt% was denoted as PSA-x. The obtained PSA/PAN FM fabricated from various concentrations of PSA/PAN was denoted as PSA/PAN-y (the weight ratio of PSA/PAN was fixed at 9:1).

Synthesis of hierarchical TiO_2@PSA/PAN FMs. Hierarchical TiO_2@PSA/PAN FMs were prepared by hydrolysis of TBT in the presence of PSA/PAN FMs in ethanol solution. First, 0.2, 0.4 and 0.8 mL of TBT were dissolved in 80 mL of absolute ethanol with magnetic stirring for 0.5 h to obtain a homogeneous mixture solution. Second, 40.0 mL of water/ethanol (volume ratio, H_2O/C_2H_5OH=1:9) mixture was added slowly to the above suspension. Third, 100 mg of PSA/PAN FM was placed in the fresh prepared solution, following transferred into a 200 mL of Teflon-lined autoclave heating at 180 °C for 12 h. Thereafter, the resultant hierarchical TiO_2@PSA/PAN FMs were washed by ethanol/water mixture (volume ratio, H_2O/C_2H_5OH=1:1) at least 5 times. The obtained product synthesized from various TBT dosages was denoted as TiO_2-z@PSA/PAN, where z stands for the dosage of TBT.

Characterization. The morphology of relevant composite fibrous membranes was examined by a scanning electron microscope (SEM, Nanolab600i) and a transmission electron microscope (TEM, JEOL JEM-1400). The sulfur element distribution of PSA/PAN emulsion was characterized by a freezing scanning electron microscope-energy dispersive X-ray (Freezing SEM-EDX, Zeiss, Sigma 500). Thermal degradation measurements were performed by thermogravimetric analysis (TGA, NETZSCH, STA 449F3). The roughness of fiber surfaces was measured by atomic force microscope (AFM, Nanoscope IV, Digital instruments). The major functional group of relevant fibrous membranes was characterized by Fourier transform infrared spectroscopy (FTIR, Spectrum One B, Perkin Elmer Inc). The near-surface chemical information of materials was analyzed by X-ray photoelectron spectroscopy (XPS, K-Alpha). The surface area and pore size distribution of the fibrous membranes were derived from N_2 ad/desorption measurements carried out at 77 K using an automatic micropore physisorption analyzer (Tristar 3020, USA). The mechanical property of relevant composite fibrous membranes was performed on a tensile tester (XQ-1C, Shanghai New Fiber Instrument Co., Ltd., China). Water contact angles (WCAs) and underwater oil contact angles (UOCAs) were performed using a contact angle goniometer (Kino SL200B). The oil content in water was detected on a total organic carbon analyser (multi N/C 2100S, Analytik Jena, Germany). The concentration of oil in water was monitored by a UV-Vis spectroscopy (UV-1800, Shimadzu). The turbidity of relevant solutions was measured by an HACH2100P turbidimeter (Hach Company, Loveland, CO, US).

Oil/Water Mixture Separation. The as-prepared membrane was fixed between two glass vessels with an effective area of 12.56 cm^2. 200 g of light oil (n-hexane)/water mixture in a volume ratio of 1:1 was poured into the upper class tube after the membrane was prewetted by water. All the separations were solely gravity driven.

Oil-in-Water Emulsion Separation. To prepare the surfactant stabilized oil-in-water emulsions, sodium dodecylbenzenesulfonate (0.1 mg/mL) was used as the emulsifier and the volume ratio of oils (n-hexane, isooctane, hexadecane, kerosene, hexane, petroleum) and water were fixed at 1:99, then the mixtures were sonicated for 1 h to produce white emulsions with an average oil droplet size of 3.75 μm (Figure S15, Supporting Information) . The membrane with an effective area of 6.25 cm^2 was fixed between the two polymethyl methacrylate (PMMA) tanks and the performance of oil-in-water emulsion separation was carried out with a vacuum driven system at 0.10 ±0.01 bar.

Supporting Information

Supporting Information is available from the Wiley Online Library or from the author.

Acknowledgements
The authors gratefully acknowledge National Natural Science Foundation of China (Grant No. 51573034), National Natural Science Foundation Project of International Cooperation (NSFC-NRF-5171101411 and NRF2017NRF-NSFC001-048), State Key Laboratory of Urban Water Resource and Environment in HIT of China (No. 2016DX14), Postdoctoral Science Foundation of Heilongjiang Prov. (No. LBH-TZ0606 and No. LBH-Q16012) and Singapore National Research Foundation (CREATE Programme of Nanomaterials for Energy and Water Management).

Received: ((will be filled in by the editorial staff))
Revised: ((will be filled in by the editorial staff))
Published online: ((will be filled in by the editorial staff))

Conflict of Interest

The authors declare no conflict of interest.

References

[1] Z. Chu, Y. Feng, S. Seeger, *Angew. Chem. Int. Edit*. **2015**, *54*, 2328.

[2] A. K. Kota, G. Kwon, W. Choi, J. M. Mabry, A. Tuteja, *Nat. Commun*. **2012**, *3*, 1025.

[3] B. Wang, W. Liang, Z. Guo, W. Liu, *Chem. Soc. Rev*. **2015**, *44*, 336.

[4] M. Tao, L. Xue, F. Liu, L. Jiang, *Adv. Mater.* **2014**, *26*, 2948.

[5] J. Song, Y. Lu, J. Luo, S. Huang, L. Wang, W. Xu, I. P. Parkin, *Adv. Mater. Interfaces* **2015**, *2*, 1500350.

[6] T. Misiti, U. Tezel, S. G. Pavlostathis, *Water Res*. **2013**, *47*, 449.

[7] W. Zhang, Z. Shi, F. Zhang, X. Liu, J. Jin, L. Jiang, *Adv. Mater.* **2013**, *25*, 2071.

[8] A. L. Ahmad, S. Ismail, S. Bhatia, *Environ. Sci. Technol*. **2005**, *39*, 2828.

[9] X. Gao, J. Zhou, R. Du, Z. Xie, S. Deng, R. Liu, Z. Liu, J. Zhang, *Adv. Mater*. **2016**, *28*, 168.

[10] J. B. Fan, Y. Song, S. Wang, J. Meng, G. Yang, X. Guo, L. Feng, L. Jiang, *Adv. Funct. Mater*. **2015**, *25*, 5368.

[11] X. Yao, J. Gao, Y. Song, L. Jiang, *Adv. Funct. Mater.* **2011**, *21*, 4270.

[12] X. Wang, J. Yu, G. Sun, B. Ding, *Mater. Today* **2016**, *19*, 403.

[13] G. Wang, Y. He, H. Wang, L. Zhang, Q. Yu, S. Peng, X. Wu, T. Ren, Z. Zeng, Q. Xue, *Green Chem.* **2015**, *17*, 3093.

[14] M. S. Islam, W. S. Choi, S. H. Kim, O. H. Han, H. J. Lee, *Adv. Funct. Mater*. **2015**, *25*, 6061.

[15] C. Cao, M. Ge, J. Huang, S. Li, S. Deng, S. Zhang, Z. Chen, K. Zhang, S. S. Al-Deyab, Y. Lai, *J. Mater. Chem. A* **2016**, *4*, 12179.

[16] Y. Gu , Y. N. Wang, J. Wei, C. Y. Tang, *Water Res*. **2013**, *47*, 1867.

[17] K. Kimura, S. Okazaki, T. Ohashi, Y. Watanabe, *J. Membr. Sci.* **2016**, *501*, 60.

[18] W. Luo, H. V Phan, M. Xie. H. F. Hai, W. E. Price, M. Elimelech, L. D. Nghiem, *Water Res*. **2017**, *109*, 122.

[19] MF. Rabuni, NMN. Sulaiman, MK. Aroua, C. Y. Chee, N. A. Hashim, *Chem. Eng. Sci*. **2015**, *122*, 426.

[20] J. Hong, Y. He, *Desalination* **2014**, *332*, 67.

[21] C. Gao, Z. Sun, K. Li, Y. Chen, Y. Cao, S. Zhang, L. Feng, *Energy Environ. Sci*. **2013**, *6*, 1147.

[22] X. Lang, W. Hao, W. R. Leow, S. Li, J. Zhao, X. Chen, *Chem. Sci.* **2015***, 6,* 5000.

[23] W. Leow, W. K. H. Ng, T. Peng, X. Liu, B. Li, W. Shi, Y. Lum, X. Wang, X. Lang, S. Li, N. Mathews, J. W. Ager, T. C. Sum, H. Hirao, X. Chen, *J. Am. Chem. Soc.* **2017**, *139*, 269.
[24] H. Fu, T. Xu, S. Zhu, Y. Zhu, *Environ. Sci. Technol*. **2008**, *42*, 8064.
[25] X. Ma, H. Li, T. Liu, S. Du, Q. Qiang, Y. Wang, S. Yin, T. Sato, *Appl. Catal. B*, **2017**, *201*, 348.
[26] J. Kim, B. Kim, C. Anand, A. Mano, Zaidi. J. S, K. Ariga, J. You, A. Vinu, E. Kim, *Angew. Chem. Int. Edit.* **2015**, *127*, 8527.
[27] F. Liu, K. Huang, Q. Wu, S. Dai, *Adv. Mater.* **2017,** *29*, 1700445.
[28] Q. Ji, X. Qiao, X. Liu, H. Jia, J. S. Yu, K. Ariga, *B. Chem. Soc. Jpn.* **2017,** *91*, 391.
[29] W. Chen, B. Xin, X. Wu, *J. Ind. Text*. **2014**, *44*, 159.
[30] Q. Xu, Q. Kong, Z. Liu, X. Wang, R. Liu, J. Zhang, L. Yue, Y. Duan, G. Cui, *ACS Sustain. Chem. Eng*. **2014**, *2*, 194.
[31] S. H. Huang, C. H. Wu, K. R. Lee, J. Y. Lai, *Appl. Mech. Mater*. **2013**, *377*, 222.
[32] J. He, W. Wang, F. Sun, W. Shi, D. Qi, K. Wang, R. Shi, C. Wang, F. Cui, X. Chen, *ACS Nano* **2015**, *9*, 9292.
[33] W. Wang, X. Lu, Z. Li, J. Lei, X. Liu, Z. Wang, H. Zhang, C. Wang, *Adv. Mater.* **2011**, *23*, 5109.
[34] Z. Zhu, Y. Liu, H. Hou, W. Shi, F. Qu, F. Cui, W. Wang, *Environ. Sci. Technol*. **2018**, *52*, 3027.
[35] Y. Si, J. Yu, X. Tang, J. Ge, B. Ding, *Nat. Commun.* **2014**, *5*, 5802.
[36] Z. Zhu, L. Zhong, Z. Zhang, H. Li, W. Shi, F. Cui, W. Wang, *J. Mater. Chem. A* **2017**, *5*, 25266.
[37] V. B. Alexander, L. Y. Alexander, M. M. Constantine, *Langmuir* **2007**, *23*, 2311.
[38] Y. Li, Z. Zhu, J. Yu, B. Ding, *ACS Appl. Mater. Interfaces* **2015**, *7*, 13538.
[39] J. Ge, Y. Si, F. Fu, J. Wang, J. Yang, L. Cui, B. Ding, J. Yu, G. Sun, *RSC Adv.* **2013**, *3*, 2248.
[40] R. N. Wenzel, *Ind. Eng. Chem*, **1936**, *28*, 988.
[41] A. B. D. Cassie, S. Baxter, *Trans. Faraday Soc*, **1944**, *40*, 546.
[42] Q. Wen, J. Di, L. Jiang, J. Yu, R. Xu, *Chem. Sci*. **2013**, *4*, 591.
[43] Q. Ma, H. Cheng, A. G. Fane, R. Wang, H. Zhang, *Small* **2016**, *12*, 2186.
[44] M. Huang, Y. Si, X. Tang, Z. Zhu, B. Ding, L. Liu, G. Zheng, W. Luo, J. Yu, *J. Mater. Chem. A* **2013**, *45*, 14071.
[45] H. Liang, W. Zhang, Y. Ma, X. Cao, Q. Guan, W. Xu, S. Yu, *ACS Nano* **2011**, *5*, 8148.
[46] S. Yang, Y. Si, Q. Fu, F. Hong, J. Yu, S. S. Al-Deyab, M. El-Newehy, B. Ding, *Nanoscale* **2014**, *6*, 12445.
[47] S. Agarwal, V. von Arnim, T. Stegmaier, H. Planck, A. Agarwal, *Sep. Purif. Technol*. **2013**, *107*, 19.
[48] P. C. Chen, Z. K. Xu, *Sci. Rep*. **2013**, *3*, 2776.

[49] X. Tang, Y. Si, J. Ge, B. Ding, L. Liu, G. Zheng, W. Luo, J. Yu, *Nanoscale* **2013**, *5*, 11657.
[50] W. Zhang, X. Lu, Z. Xin, C. Zhou, *Nanoscale* **2015**, *7*, 19476.
[51] M. Hu, S. Zheng, B. Mi, *Environ. Sci. Technol*. **2016**, *50*, 685.
[52] R. Zhang, Y. Liu, M. He, Y. Su, X. Zhao, M. Elimelech, Z. Jiang, *Chem. Soc. Rev*. **2016**, *45*, 5888.
[53] Y. Ye, P. Le Clech, V. Chen, A. G. Fane, B. Jefferson, *Desalination* **2005**, *175*, 7.
[54] Z. Chu, Y. Feng, S. Seeger, *Angew. Chem. Int. Ed*. **2015**, *54*, 2328.
[55] Y. Zhu, D. Wang, L. Jiang, J. Jin, *NPG Asia Mate*r. **2014**, *6*, e101.
[56] J. S. Lintuvuori, K. Stratford, M. E. Cates, D. Marenduzzo, *Phys. Rev. Lett*. **2010**, *105*, 178302.

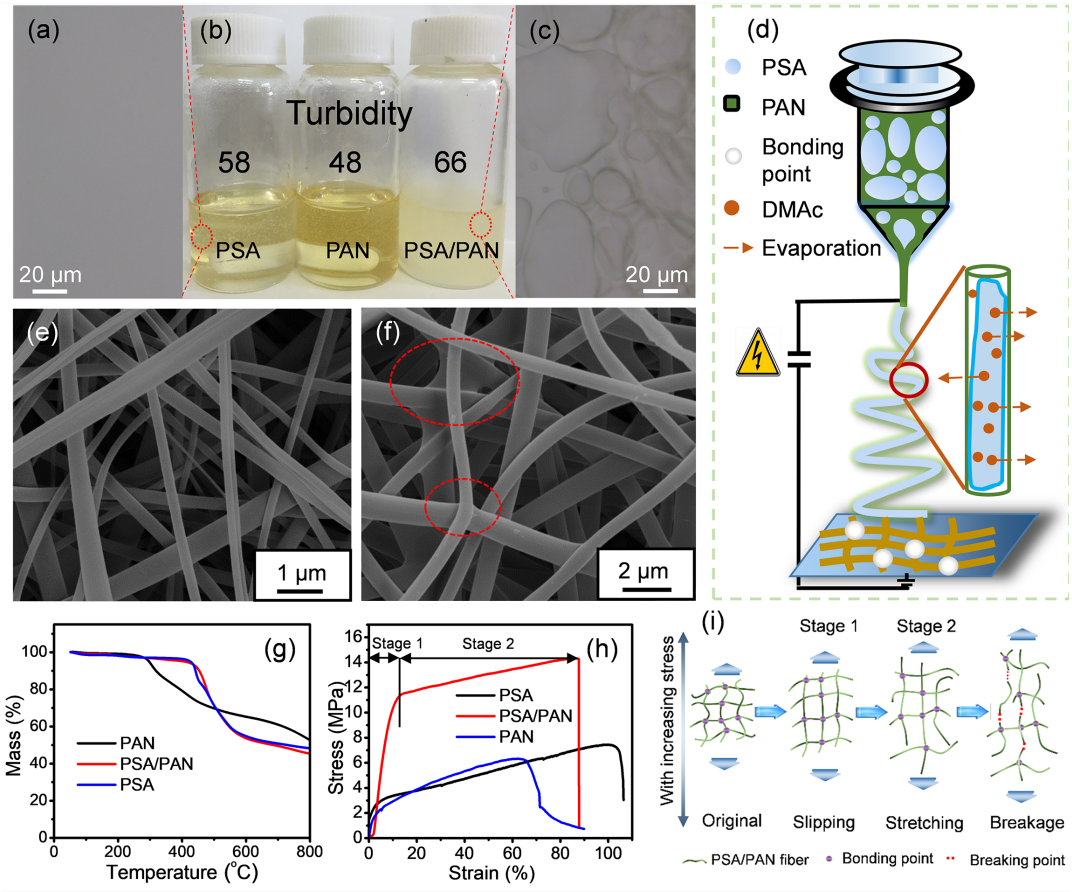

Figure 1. Optical micrographs of (a) PSA and (c) PSA/PAN solution. (b) Photograph of the relevant solutions, the numbers indicating the turbidity of relevant solutions. (d) Schematic diagram illustrating the *in situ* generation mechanism of the bonding structured fibrous membrane. (e) SEM images of PSA (22 wt%) and (f) PSA/PAN (PSA/PAN=9/1, 14 wt%) fibers. (g) TG and (h) stress-strain curves of the as-prepared PSA, PSA/PAN and PAN FMs. (i) Break mechanism of the bonding structured fibrous membrane.

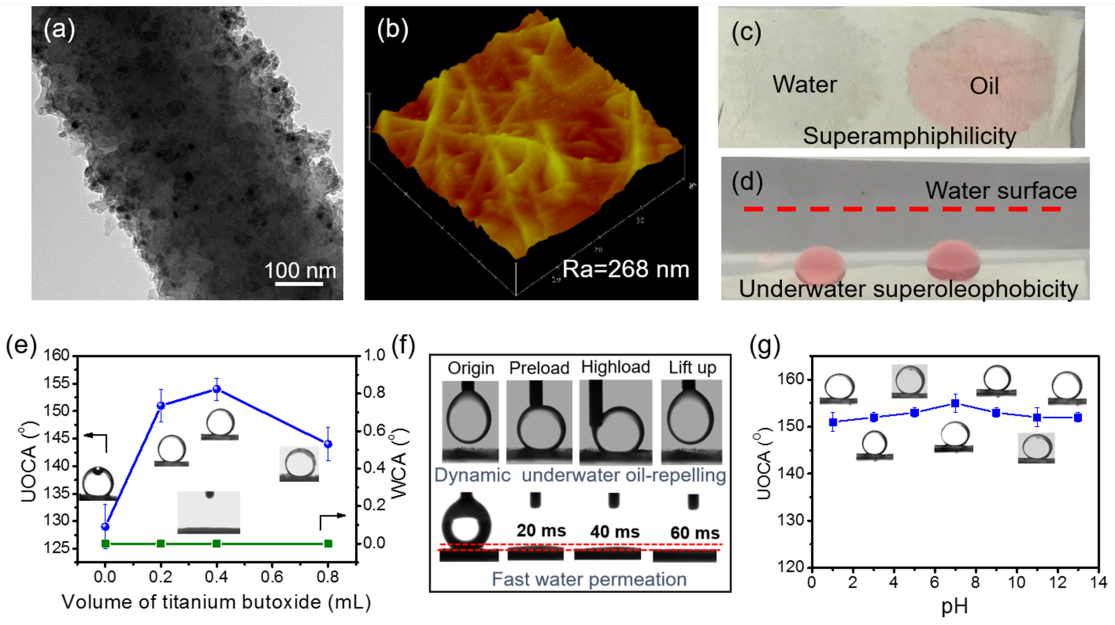

Figure 2. (a) TEM and (b) AFM images of the hierarchical TiO_2-0.4@PSA/PAN FM. (c) Water and oil droplets dyed with Sudan red G on the TiO_2-0.4@PSA/PAN FM in air. (d) Photograph of underwater oil droplets (3 μL) on the TiO_2-0.4@PSA/PAN fibrous membrane surface. (e) Variations of the UOCAs and the corresponding optical profiles of oil droplets on the hierarchical TiO_2-0.4@PSA/PAN FM. (f) Photographs of underwater oil-repelling and dynamic measurements of water permeation on the TiO_2-0.4@PSA/PAN fibrous membrane surface. (g) The relationship between the pH and the UOCAs of TiO_2-0.4@PSA/PAN fibrous membrane surface.

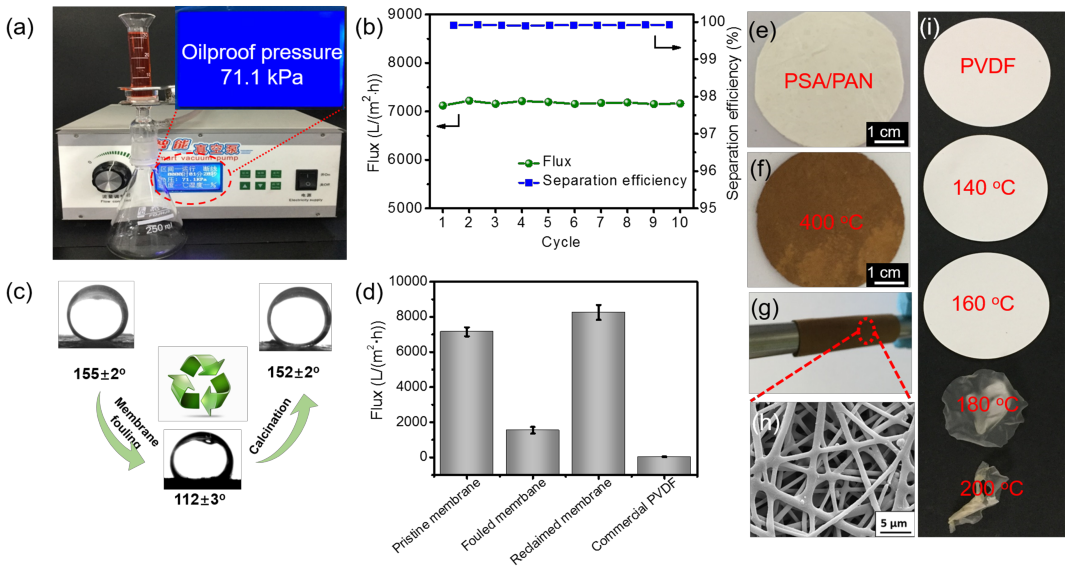

Figure 3. (a) Photograph showing the oil proof pressure of TiO_2-0.4@PSA/PAN FM measured *via* a controllable vacuum pump. (b) Changes of the water flux with increasing separation cycles of oil/water mixture using TiO_2-0.4@PSA/PAN FM. (c) UOCA images showing the thermal reclamation process of the fouled TiO_2-0.4@PSA/PAN FM annealing treated at 400 °C. (d) A comparison between fluxes of pristine, fouled, and revived membranes and commercial PVDF membrane. Photographs of (e) the as-prepared and (f) the post-annealing TiO_2-0.4@PSA/PAN FMs. (g) Photographs showing the flexibility and (h) SEM image of the fouled TiO_2-0.4@PSA/PAN FM after annealing treatment. (i) Photographs of the commercial hydrophilic PVDF membranes exposed to various temperatures in air.

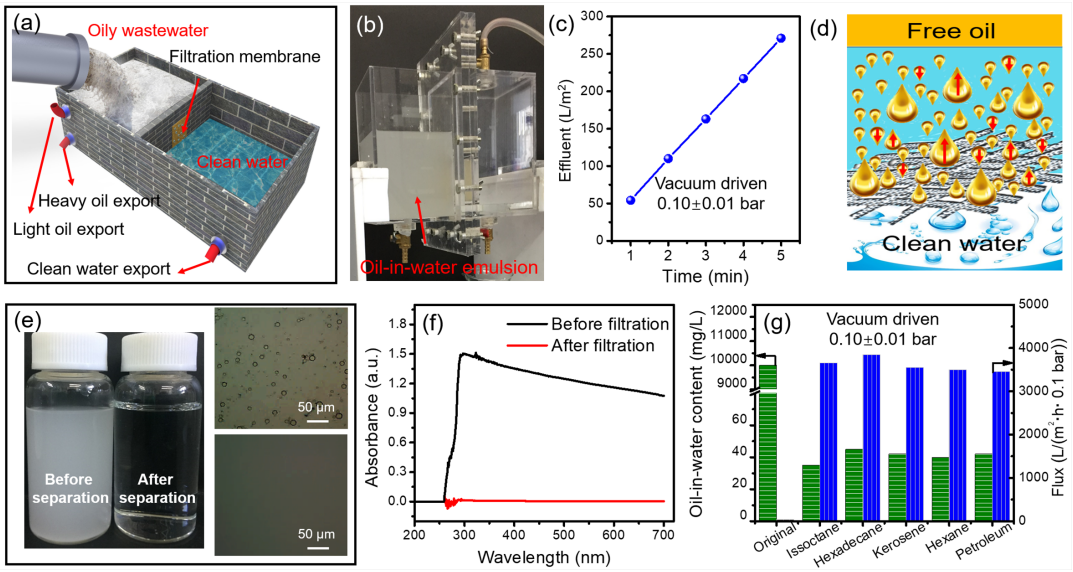

Figure 4. (a) Schematic diagram showing the separation device in real application. (b) Photograph showing the self-made separation equipment in operation. (c) Amount of effluent collected with increasing time during oil-in-water emulsion separation using TiO_2-0.4@PSA/PAN FM. (d) Schematic diagram illustrating a plausible mechanism of the oil-in-water emulsion separation. (e) Digital images and micrographs of SDBS stabilized n-hexane-in-water emulsion and the filtrate. (f) The UV–vis spectra of the as-prepared oil-in-water emulsion and the filtrate. (g) The water flux and the separation efficiency for various oil-in-water emulsions using TiO_2-0.4@PSA/PAN FM.

TOC

A calcinable polymer membrane with revivablility was rationally designed for oily water remediation. The inter-bonding structured TiO_2@PSA/PAN fibrous membrane exhibited a high water flux, excellent separation efficiency and robust thermal stability (400 °C). More importantly, the fouled membrane could be easily reclaimed without decrease in separation performance and mechanical property by annealing treatment.

Keywords: Calcinable polymer membrane; revivable membrane; oily water remediation; composite materials; electrospinning

Zhigao Zhu, Wei Wang*, Dianpeng Qi, Yifei Luo, Yuanren Liu, Ying Xu, Fuyi Cui, Ce Wang, Xiaodong Chen*

Calcinable Polymer Membrane with Revivability for Efficient Oily Water Remediation